Parton distributions of intrinsic charm in two-dimensional QCD

Siwei Hu,[1,2,*] Yu Jia,[1,2,†] Zhewen Mo,[1,2,‡] Xiaonu Xiong,[3,§] and Mingliang Zhu[3,‖]
[1]*Institute of High Energy Physics, Chinese Academy of Sciences, Beijing 100049, China*
[2]*School of Physics, University of Chinese Academy of Sciences, Beijing 100049, China*
[3]*School of Physics, Central South University, Changsha 418003, China*

(Received 5 September 2023; accepted 12 October 2023; published 29 November 2023)

We present a detailed investigation on the intrinsic charm content in a light meson within the 't Hooft model, namely, two-dimensional QCD in the large-N_c limit. The intrinsic charm parton distribution function (PDF) of a light meson, which first arises at order N_c^{-1}, is explicitly expressed in terms of the 't Hooft wave functions of the light meson and an infinite tower of excited charmed mesons. We also derive the functional forms of the two-dimensional counterparts of the meson cloud model and Brodsky-Hoyer-Peterson-Sakai model. We then make a quantitative comparison between our results and model predictions. We also study how the profile of the intrinsic charm PDF varies with charm-quark mass. The average momentum fraction carried by the charm quark inside a light meson is found to decrease as m_c^{-6} in the heavy charm quark mass limit.

DOI: 10.1103/PhysRevD.108.094040

I. INTRODUCTION

The probability distributions of the momenta carried by light quarks and gluons inside a nucleon, namely, the parton distribution functions (PDFs), are the key nonperturbative ingredients to unravel the internal structure of the nucleon. In the past half century, the nucleon PDF has been determined with very high precision from numerous high-energy collision experiments [1]. Although the nucleon is viewed as a baryon composed of three light quarks in the context of the naive quark model, it is generally believed that it must contain higher Fock components that entail heavy quark and antiquark pairs, e.g., $|uudc\bar{c}\rangle$, due to ubiquitous quantum fluctuation. It has long been envisaged that the nucleon may have a non-negligible charm content, usually dubbed *intrinsic* charm [2–4]. Due to its nonperturbative nature, the intrinsic charm should be distinguished from the *extrinsic* charm, which actually emerges from gluon splitting according to Dokshitzer-Gribov-Lipatov-Altarelli-Parisi evolution. It has often been warned that the exact interpretation of intrinsic charm may suffer from some ambiguity. For the notion of the intrinsic charm to make sense, the lifetime of an intrinsic $c\bar{c}$ pair inside a nucleon must be much longer than the typical interaction time in the deep-inelastic scattering processes [5].

Recently, the NNPDF Collaboration released an analysis of the latest LHCb experimental data [6] on Z-boson production associated with a charm jet. They claimed that the LHCb data can be decently accommodated (at a significance level of 3σ [7]) only after including the intrinsic charm PDF in the analysis. This result may indicate that the existence of a charm component in the proton is non-negligible. We note that some time ago the CTEQ-TEA global analysis [1] placed an upper bound on the average charm momentum fraction in a proton, which is less than 2% or 1.6% at the renormalization scale $\mu = 1.3$ GeV. The recent NNPDF analysis indicated that the average momentum fraction carried by the nonperturbative charm is $0.62\% \pm 0.28\%$ at $\mu = 1.65$ GeV [7]. Nevertheless, the NNPDF analysis has not been universally accepted, and there is some ongoing debate on the existence of intrinsic charm content reported by the NNPDF Collaboration [8,9].

It is very challenging to investigate the intrinsic charm PDF in a light hadron directly from the first principles of QCD [10]. The charm-anticharm asymmetry[1] in the nucleon is constrained by a combined analysis from QCD model and

*husw@ihep.ac.cn
†jiay@ihep.ac.cn
‡mozw@ihep.ac.cn
§xnxiong@csu.edu.cn
‖lightzhu@csu.edu.cn

[1]In this work, we only focus on the intrinsic charm PDF of quarkonia, which is a flavor-neutral system with definite C parity. Thus the charm-anticharm asymmetry cannot emerge from this system. To study a nonvanishing charm-anticharm asymmetry, one must pursue the flavored meson which is beyond the scope of this work.

lattice-calculated form factors [11]. The large momentum effective theory [12–14] may have the potential to directly calculate the x dependence of the intrinsic charm PDF on the lattice in the future. However, currently one has to resort to phenomenological models to parametrize the intrinsic charm PDF in a nucleon. Two popular models are the meson cloud model (MCM) [15–17] and Brodsky-Hoyer-Peterson-Sakai (BHPS) model [2,3].

Needless to say, it is highly desirable to understand the intrinsic charm PDF from a first-principles perspective. Although seemingly formidable, it is actually possible to achieve this goal in some toy models of QCD. In this work, we attempt to investigate the intrinsic charm content of a light meson in $1+1$-dimensional QCD in the large-N_c limit, which was originally introduced by 't Hooft in 1974 [18]. Despite being a simple solvable model, the 't Hooft model resembles realistic QCD in several aspects, e.g., color confinement, Regge trajectory, and chiral condensate. A notable simplification in QCD_2 is the lack of a dynamic gluon. Once imposing light-cone gauge, the gluonic degree of freedom descends simply to an inter-quark potential. The 't Hooft model thus may serve as an ideal theoretical laboratory to study the intrinsic charm PDF of a light hadron. The aim of this work is to rigorously deduce the functional form of the intrinsic charm PDF inside a light meson in this toy model, which starts at order $1/N_c$. To make a comparison, we also present the intrinsic charm PDF predicted by the light-front two-dimensional counterparts of the BHPS model and MCM. It should be pointed out beforehand that QCD_2 still differs from the realistic QCD_4 in some aspects, e.g., the transverse degree of freedom is absent in QCD_2 and there is no dynamical gluon in some noncovariant gauges such as the light-cone gauge. Thus, one may expect that the intrinsic charm distributions are different in QCD_2 and QCD_4. For instance, the scaling of Mellin moments with respect to charm-quark mass is m_c^{-2} [19] in realistic QCD_4, while we found that the scaling is approximately m_c^{-6} in QCD_2 (see Sec. V for details). This work may provide some novel insight for the understanding of the origin of the intrinsic charm component inside a light hadron from the field-theoretical perspective. In this solvable toy model, we also explicitly point out the similarity and difference between our field-theoretical approach and some influential phenomenological models such as the MCM. We hope that the lessons learned from this toy model may be useful to better understand the intrinsic charm content of the PDF in realistic QCD.

The rest of this paper is organized as follows. In Sec. II we briefly review the Hamiltonian formalism of the 't Hooft model in the $N_c \to \infty$ limit. In Sec. III we extend the formalism to the next-to-leading order in $1/N_c$, and construct the functional form of the intrinsic charm PDF with the aid of first-order quantum-mechanical perturbation theory. In Sec. IV we give the explicit expressions of the intrinsic charm PDF within the two-dimensional versions of the BHPS model and MCM. We also discuss the relation between our results and the MCM result. We devote Sec. V to comprehensive numerical studies of the intrinsic charm PDF in a light meson which are calculated using various approaches. We also study how the first and second Mellin moments of the intrinsic charm PDF vary with increasing charm mass. Finally, we summarize in Sec. VI.

II. A BRIEF REVIEW OF THE HAMILTONIAN APPROACH IN THE 'T HOOFT MODEL

In this section, we briefly review how to derive the 't Hooft equation using the light-front Hamiltonian method. For more details, we refer interested readers to Ref. [20]. The QCD Lagrangian in two spacetime dimensions reads

$$\mathcal{L} = -\frac{1}{4}F^{a,\mu\nu}F^{a}_{\mu\nu} + \sum_f \bar{\psi}_f(i\not{D} - m_f)\psi_f, \tag{1}$$

where $D_\mu = \partial_\mu - ig_s A^a_\mu T^a$ signifies the color-covariant derivative and T^a denotes the generators of the $SU(N_c)$ group in the fundamental representation. The gluon field-strength tensor is defined as $F^a_{\mu\nu} \equiv \partial_\mu A^a_\nu - \partial_\nu A^a_\mu + g_s f^{abc} A^b_\mu A^c_\nu$. f denotes the flavor of quarks. In this work, we concentrate on the two-flavor case, where f can be either the up or charm quark. We use the chiral-Weyl representation for the Dirac γ matrices,

$$\gamma^0 = \sigma_1, \qquad \gamma^z = -i\sigma_2, \qquad \gamma_5 \equiv \gamma^0\gamma^z = \sigma_3, \tag{2}$$

and the Dirac spinor field in this representation is

$$\psi = 2^{-\frac{1}{4}}\begin{pmatrix}\psi_R \\ \psi_L\end{pmatrix}, \tag{3}$$

where R, L denote the right-handed and left-handed components, respectively.

The chiral limit and $N_c \to \infty$ limit do not generally commute. In this work, we specify the 't Hooft model in the so-called "weak-coupling" limit:

$$N_c \to \infty, \qquad \lambda \equiv \frac{g_s^2 N_c}{4\pi}\,\text{fixed}, \qquad m_q \gg g_s \sim \frac{1}{\sqrt{N_c}}, \tag{4}$$

where λ of mass dimension two denotes the 't Hooft coupling constant. We assume the up quark to be light, so $m_u \leq \sqrt{2\lambda}$, while the charm quark is regarded as heavy, and hence $m_c \gg \sqrt{2\lambda}$.

It is convenient to adopt the light-cone coordinates $x^\pm = x_\mp = (x^0 \pm x^z)/\sqrt{2}$. Substituting (3) into (1), and imposing the light-cone gauge $A^{+,a} = 0$, one obtains [18]

$$\mathcal{L} = \frac{1}{2}(\partial_- A^{-,a})^2 + g_s \psi^\dagger_{f,R} A^{-,a} T^a \psi_{f,R} + \psi^\dagger_{f,R} i\partial_+ \psi_{f,R} + \psi^\dagger_{f,L} i\partial_- \psi_{f,L} - \frac{m_f}{\sqrt{2}}\left(\psi^\dagger_{f,L}\psi_{f,R} + \psi^\dagger_{f,R}\psi_{f,L}\right), \tag{5}$$

where the flavor index f is summed over u and c.

In the light-cone gauge, $A^{-,a}$ and ψ_L are no longer the dynamical variables. From the equations of motion, they can be expressed in terms of the canonical variable ψ_R (the "good" component):

$$\partial_-^2 A^{-,a} - g_s \psi^\dagger_R T^a \psi_R = 0, \tag{6a}$$

$$i\partial_- \psi_L - \frac{m}{\sqrt{2}}\psi_R = 0. \tag{6b}$$

Substituting the solutions of these two equations into the light-front (LF) Hamiltonian, we obtain

$$\begin{aligned} H_{\mathrm{LF}} = P^- = \int_{x^+=\mathrm{const}} dx^- \Bigg[& \frac{m^2}{2i}\psi^\dagger_R(x^-) \\ & \times \int dy^- G^{(1)}(x^- - y^-)\psi_R(y^-) \\ & - \frac{g_s^2}{2}\sum_a \psi^\dagger_R(x^-) T^a \psi_R(x^-) \\ & \times \int dy^- G^{(2)}(x^- - y^-)\psi^\dagger_R(y^-) T^a \psi_R(y^-)\Bigg], \end{aligned} \tag{7}$$

where $G^{(1)}$ and $G^{(2)}$ are the Green functions affiliated with the differential operators ∂_- and ∂_-^2:

$$G^{(1)}(x^- - y^-) = i\int \frac{dk^+}{2\pi}\Theta(|k^+| - \rho)\frac{e^{-ik^+(x^- - y^-)}}{k^+}, \tag{8a}$$

$$G^{(2)}(x^- - y^-) = -\int \frac{dk^+}{2\pi}\Theta(|k^+| - \rho)\frac{e^{-ik^+(x^- - y^-)}}{(k^+)^2}. \tag{8b}$$

Here ρ is an artificial IR cutoff introduced to regularize the divergence caused by exchanging an instantaneous gluon.

The quark fields are quantized using the light-front formalism (Dirac's front form)

$$\{\psi^i_R(x^+, x^-), \psi^{j\dagger}_R(y^+, y^-)\}|_{x^+=y^+} = \delta^{ij}\delta(x^- - y^-), \tag{9a}$$

$$\begin{aligned} & \{\psi^i_R(x^+, x^-), \psi^j_R(y^+, y^-)\}|_{x^+=y^+} \\ & = \{\psi^{i\dagger}_R(x^+, x^-), \psi^{j\dagger}_R(y^+, y^-)\}|_{x^+=y^+} = 0, \end{aligned} \tag{9b}$$

where i, j denote the color indices. The quark field can be further expanded using the annihilation and creation operators

$$\psi^i_R = \int_0^\infty \frac{dk^+}{2\pi}[b^i(k^+)e^{-ik^+x^-} + d^{i\dagger}(k^+)e^{ik^+x^-}]. \tag{10}$$

One important feature of the 't Hooft model is the color confinement. The isolated quarks and antiquarks cannot manifest themselves in a physical spectrum. It is the color-neutral quark-antiquark pair that can be created or annihilated in a physical process. The technique of bosonization [21–28] turns out to be useful to diagonalize the light-front Hamiltonian. One can define a set of color-singlet compound operators M, B, and D from the quark/antiquark creation and annihilation operators:

$$M^{\bar{f}_1 f_2}(k^+, p^+) = \frac{1}{\sqrt{N_c}}\sum_c d^{c,f_1}(k^+)b^{c,f_2}(p^+), \tag{11a}$$

$$\begin{aligned} B^{f_1,f_2}(k^+, p^+) &= \sum_c b^{c,f_1\dagger}(k^+)b^{c,f_2}(p^+) \\ &\to \int_0^\infty \frac{dq^+}{2\pi}\sum_{f_i} M^{\dagger \bar{f}_i f_1}(q^+, k^+)M^{\bar{f}_i f_2}(q^+, p^+), \end{aligned} \tag{11b}$$

$$\begin{aligned} D^{\bar{f}_1,\bar{f}_2}(k^+, p^+) &= \sum_c d^{c,f_1\dagger}(k^+)d^{c,f_2}(p^+) \\ &\to \int_0^\infty \frac{dq^+}{2\pi}\sum_{f_i} M^{\dagger \bar{f}_1 f_i}(k^+, q^+)M^{\bar{f}_2 f_i}(p^+, q^+), \end{aligned} \tag{11c}$$

where c denotes the color index. The last equations reflect the color confinement assumption.

The commutation relation between M and $M^\dagger$ is given by

$$\begin{aligned} & [M^{\bar{f}_1 f_2}(k_1^+, p_1^+), M^{\dagger \bar{f}_3 f_4}(k_2^+, p_2^+)] \\ & = (2\pi)^2 \delta_{f_1 f_3}\delta_{f_2 f_4}\delta(k_1^+ - k_2^+)\delta(p_1^+ - p_2^+) + \mathcal{O}\left(\frac{1}{N_c}\right), \end{aligned} \tag{12}$$

and all other commutators among M, B, D are at order $\mathcal{O}(1/N_c)$. Since baryons become infinitely heavy and decouple in the $N_c \to \infty$ limit, mesons are the only physical color-singlet states in this model. One can diagonalize the light-front Hamiltonian by trading the compound operators M and $M^\dagger$ for the mesonic annihilation and creation operators m_n and $m_n^\dagger$ (where n signifies the nth excited meson). These two sets of operators are related by the following relations:

$$M^{\bar{f}_1 f_2}((1-x)P^+, xP^+) = \sqrt{\frac{2\pi}{P^+}}\sum_{n=0}^\infty \varphi_n^{f_2 \bar{f}_1}(x) m_n^{f_2 \bar{f}_1}(P^+), \tag{13a}$$

$$m_n^{f_1\bar{f}_2}(P^+) = \sqrt{\frac{P^+}{2\pi}} \int_0^1 dx \varphi_n^{f_1\bar{f}_2}(x) M^{\bar{f}_2 f_1}((1-x)P^+, xP^+), \tag{13b}$$

where the coefficient function $\varphi_n^{f_1\bar{f}_2}(x)$ is interpreted as the light-cone ('t Hooft) wave function of the nth excited meson with the flavor content $f_1\bar{f}_2$.

The meson annihilation and creation operators are assumed to obey the standard commutation relation:

$$[m_n^{f_i\bar{f}_j}(P_1^+), m_r^{\dagger f_k\bar{f}_l}(P_2^+)] = 2\pi\delta_{f_i f_k}\delta_{f_j f_l}\delta_{nr}\delta(P_1^+ - P_2^+) + \mathcal{O}\left(\frac{1}{N_c}\right). \tag{14}$$

In order to have the desired commutation relation in (14), the 't Hooft wave functions must satisfy the following orthogonality and completeness conditions:

$$\int_0^1 dx\, \varphi_n^{f_1\bar{f}_2}(x)\varphi_m^{f_1\bar{f}_2}(x) = \delta_{nm}, \tag{15}$$

$$\sum_n \varphi_n^{f_1\bar{f}_2}(x)\varphi_n^{f_1\bar{f}_2}(y) = \delta(x-y). \tag{16}$$

At the leading order in $1/N_c$, the light-front Hamiltonian is simply a free Hamiltonian composed of all possible meson states:

$$H_{\mathrm{LF}} = P^- = H_{\mathrm{vac}} + \sum_{n,f_1f_2} \int \frac{dP^+}{2\pi} P^-_{n,f_1f_2} m_n^{\dagger f_1\bar{f}_2}(P^+) \times m_n^{f_1\bar{f}_2}(P^+) + \mathcal{O}\left(\frac{1}{\sqrt{N_c}}\right). \tag{17}$$

The exact form of the vacuum energy H_{vac} can be found in [20] and H_{vac} is a constant which does not have any physical effect in this work. In order to reach such a diagonalized Hamiltonian, the meson light-cone wave function must obey the celebrated 't Hooft equation [18]:

$$\left(\frac{m_1^2}{x} + \frac{m_2^2}{1-x}\right)\varphi_n^{f_1\bar{f}_2}(x) - 2\lambda \fint_0^1 dy \frac{\varphi_n^{f_1\bar{f}_2}(y) - \varphi_n^{f_1\bar{f}_2}(x)}{(x-y)^2} = \mu^2_{n,f_1,f_2}\varphi_n^{f_1\bar{f}_2}(x), \tag{18}$$

where m_1, m_2 are the current-quark masses affiliated with flavor f_1 and f_2, respectively, and μ^2_{n,f_1f_2} is the squared meson mass. The symbol $\fint$ denotes the principal value prescription for an integral, defined as

$$\fint dy \frac{f(y)}{(x-y)^2} = \lim_{\epsilon\to 0^+} \int dy \Theta(|x-y|-\epsilon)\frac{f(y)}{(x-y)^2} - \frac{2f(x)}{\epsilon}. \tag{19}$$

Note that the IR regulator ρ finally disappears from the LF Hamiltonian (17) as well as the 't Hooft equation, as it should.

III. INTRINSIC CHARM PDF OF A LIGHT MESON

Let us consider a light neutral meson composed of the u and $\bar{u}$ quarks. For notational brevity, we simply call it π. The intrinsic charm PDF of a pion follows the standard Collins-Soper definition [29]:

$$f_{c/\pi}(x) = \int \frac{dz^-}{4\pi} e^{-ixP^+z^-} \left\langle \pi(P^+)|\bar{c}(z^-)\gamma^+ \mathcal{P}\left[\exp\left(-ig_s\int_0^{z^-} d\eta^- A^+(\eta^-)\right)\right] c(0)|\pi(P^+)\right\rangle_{\mathrm{connected}}, \tag{20}$$

where P^+ is the $+$ momentum of the pion and x is the frame-independent light-front momentum fraction $k^+/P^+ = (k^0+k^z)/(P^0+P^z)$ carried by the charm quark with respect to the meson. c and $\bar{c}$ denote the charm quark fields, and $\mathcal{P}[\cdots]$ denotes the gauge link which ensures the gauge invariance of the PDF. Since we have worked with the light-cone gauge $A^{a,+} = 0$, the gauge link can thus be simply dropped.

Employing the bosonization technique as mentioned in the preceding section, the color-singlet nonlocal charm quark bilinear in (20) can be expressed in terms of the mesonic creation and annihilation operators:

$$\begin{aligned}\bar{c}(z^-)\gamma^+ c(0) &= c_R^\dagger(z^-)c_R(0) \\ &= \int \frac{dk_1^+ dk_2^+}{2\pi} N_c \delta(k_1^+ - k_2^+) e^{-ik_1^+ z^-} \\ &\quad + \sum_n \int \frac{dk_1^+ dk_2^+}{(4\pi)^{3/2}} \frac{\sqrt{N_c}}{\sqrt{k_1^+ + k_2^+}} e^{ik_1^+ z^-} m_n^{\dagger c\bar{c}}(k_1^+ + k_2^+)\varphi_n^{c\bar{c}}\left(\frac{k_1^+}{k_1^+ + k_2^+}\right)\end{aligned}$$

$$+\sum_n \int \frac{dk_1^+ dk_2^+}{(4\pi)^{3/2}} \frac{\sqrt{N_c}}{\sqrt{k_1^+ + k_2^+}} e^{-ik_1^+ z^-} m_n^{c\bar{c}}(k_1^+ + k_2^+) \varphi_n^{c\bar{c}}\left(\frac{k_2^+}{k_1^+ + k_2^+}\right)$$
$$+\sum_{f,n_1 n_2} \int \frac{dk_1^+ dk_2^+ dq^+}{(2\pi)^2} e^{ik_1^+ z^-} m_{n_1}^{\dagger c\bar{f}}(k_1^+ + q^+) m_{n_2}^{c\bar{f}}(k_2^+ + q^+) \frac{\varphi_{n_1}^{c\bar{f}}\left(\frac{k_1^+}{k_1^+ + q^+}\right)}{\sqrt{k_1^+ + q^+}} \frac{\varphi_{n_2}^{c\bar{f}}\left(\frac{k_2^+}{k_2^+ + q^+}\right)}{\sqrt{k_2^+ + q^+}}$$
$$-\sum_{f,n_1 n_2} \int \frac{dk_1^+ dk_2^+ dq^+}{(2\pi)^2} e^{-ik_1^+ z^-} m_{n_1}^{\dagger f\bar{c}}(k_2^+ + q^+) m_{n_2}^{f\bar{c}}(k_1^+ + q^+) \frac{\varphi_{n_1}^{f\bar{c}}\left(\frac{q^+}{k_2^+ + q^+}\right)}{\sqrt{k_2^+ + q^+}} \frac{\varphi_{n_2}^{f\bar{c}}\left(\frac{q^+}{k_1^+ + q^+}\right)}{\sqrt{k_1^+ + q^+}}. \tag{21}$$

The $\mathcal{O}(N_c)$ term contributes to the disconnected part, and thus can be dropped. The $\mathcal{O}(\sqrt{N_c})$ terms only contain a single meson creation or annihilation operator, which also yields a null contribution when sandwiched between two π states. Only the last two terms of $\mathcal{O}(N_c^0)$ yield nonvanishing contributions, which represent the charmed meson sector and anticharmed meson sector, respectively.

Next we turn to the higher Fock component inside a physical π state. In the $N_c \to \infty$ limit, the π only contains the valence constituents $u\bar{u}$. In order to nail down its intrinsic charm content, one has to expand the QCD_2 light-front Hamiltonian to next-to-leading order in $1/N_c$. Let us split the full Hamiltonian into $H_{\mathrm{LF}} = H_{\mathrm{LF},0} + V$, where the free mesonic Hamiltonian $H_{\mathrm{LF},0}$ is given in (17), and the V term encapsulates all possible $\mathcal{O}(1/\sqrt{N_c})$ three-meson interactions. Invoking the first-order quantum-mechanical perturbation theory, the physical pion state can be expressed as

$$|\pi'\rangle \approx |\pi\rangle + \frac{1}{P^- - H_{\mathrm{LF},0} + i\epsilon} V|\pi\rangle. \tag{22}$$

$|\pi'\rangle$ denotes the eigenstate of the full Hamiltonian, and $|\pi\rangle$ signifies the eigenstate of $H_{\mathrm{LF},0}$, which can be generated by

$$|\pi_n(P^+)\rangle = \sqrt{2P^+} m_n^{\dagger u\bar{u}}(P^+)|0\rangle, \tag{23}$$

where n denotes the principle quantum number.

It is well known that the $\mathcal{O}(1/\sqrt{N_c})$ piece of the interaction potential V is governed by a three-meson coupling [30]. For our concern, the most relevant parts in V are those coupling π with all possible charmed mesons and anticharmed mesons:

$$V_{\mathrm{charm}} = \mathcal{V} + \bar{\mathcal{V}} + \mathrm{H.c.}, \tag{24}$$

where

$$\mathcal{V} = \frac{-\lambda}{(2\pi)^{\frac{3}{2}}\sqrt{N_c}} \sum_{n_1 n_2 n_3} \int_0^\infty dq^+ dk_1^+ dk_2^+ dk_3^+ dk_4^+ \delta(k_1^+ - k_2^+ + k_3^+ + k_4^+) m_{n_1}^{\dagger c\bar{u}}(k_1^+ + q^+) m_{n_2}^{u\bar{u}}(k_2^+ + q^+) m_{n_3}^{\dagger u\bar{c}}(k_3^+ + k_4^+)$$
$$\times \frac{1}{(k_3^+ - k_2^+)^2} \frac{\varphi_{n_1}^{c\bar{u}}\left(\frac{k_1^+}{k_1^+ + q^+}\right)}{\sqrt{k_1^+ + q^+}} \frac{\varphi_{n_2}^{u\bar{u}}\left(\frac{k_2^+}{k_2^+ + q^+}\right)}{\sqrt{k_2^+ + q^+}} \frac{\varphi_{n_3}^{u\bar{c}}\left(\frac{k_3^+}{k_3^+ + k_4^+}\right)}{\sqrt{k_3^+ + k_4^+}}, \tag{25a}$$

$$\bar{\mathcal{V}} = \frac{\lambda}{(2\pi)^{\frac{3}{2}}\sqrt{N_c}} \sum_{n_1 n_2 n_3} \int_0^\infty dq^+ dk_1^+ dk_2^+ dk_3^+ dk_4^+ \delta(k_1^+ - k_2^+ + k_3^+ + k_4^+) m_{n_1}^{\dagger u\bar{c}}(k_1^+ + q^+) m_{n_2}^{u\bar{u}}(k_2^+ + q^+) m_{n_3}^{\dagger c\bar{u}}(k_3^+ + k_4^+)$$
$$\times \frac{1}{(k_3^+ - k_2^+)^2} \frac{\varphi_{n_1}^{u\bar{c}}\left(\frac{q^+}{k_1^+ + q^+}\right)}{\sqrt{k_1^+ + q^+}} \frac{\varphi_{n_2}^{u\bar{u}}\left(\frac{q^+}{k_2^+ + q^+}\right)}{\sqrt{k_2^+ + q^+}} \frac{\varphi_{n_3}^{c\bar{u}}\left(\frac{k_4^+}{k_3^+ + k_4}\right)}{\sqrt{k_3^+ + k_4^+}}. \tag{25b}$$

Note that V_{charm} is indeed of order $1/\sqrt{N_c}$. Obviously, the interaction potential V_{charm} can induce transitions from π into a $D\bar{D}$ pair, with D and $\bar{D}$ generically referring to all possible excited charmed and anticharmed mesons.

To proceed, let us insert a complete set of hadronic states in the left of V_{charm} into Eq. (22). Clearly, only those intermediate states composed of free $D\bar{D}$ pairs can survive in the sum. Equation (22) can then be recast as

$$|\pi_n'(P^+)\rangle \approx |\pi_n(P^+)\rangle + \sum_{n_i n_j} \int_0^\infty \frac{dk_i^+ dk_j^+}{(2\pi)^2 2k_i^+ 2k_j^+} \tilde{T}_{n,n_i,n_j}(k_i^+, k_j^+)|D_{n_i}(k_i^+)\bar{D}_{n_j}(k_j^+)\rangle, \tag{26}$$

where the completed charmed hadronic states arising from the first-order perturbation are defined by

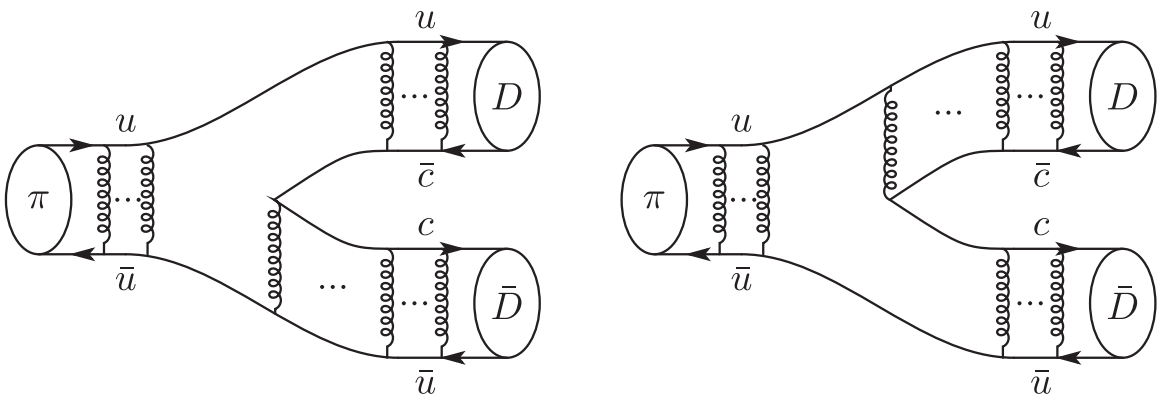

FIG. 1. Schematic diagrams illustrating a pion transitioning into a $D\bar{D}$ pair.

$$|D_{n_i}(k_i^+), \bar{D}_{n_j}(k_j^+)\rangle = 2\sqrt{k_i^+ k_j^+}\, m_{n_i}^{\dagger c\bar{u}}(k_i^+) m_{n_j}^{\dagger u\bar{c}}(k_j^+)|0\rangle. \tag{27}$$

For the sake of generality, here we consider the intrinsic charm content of the nth excited pion state (denoted by π_n), rather than only the ground-state π. The $\tilde{T}$ function in (26) is defined as

$$\begin{aligned}\tilde{T}_{n,n_i,n_j}(k_i^+, k_j^+) &\equiv \langle D_{n_i}(k_i^+)\bar{D}_{n_j}(k_j^+)|\pi_n'(P^+)\rangle \\ &\approx \langle D_{n_i}(k_i^+)\bar{D}_{n_j}(k_j^+)|V_{\text{charm}}|\pi_n(P^+)\rangle \\ &\quad\times\left(\frac{\mu_{D_{n_i}}^2}{2k_i^+}+\frac{\mu_{\bar{D}_{n_j}}^2}{2k_j^+}-\frac{\mu_{\pi_n}^2}{2P^+}\right)^{-1}.\end{aligned} \tag{28}$$

This function has a clear physical interpretation, which characterizes the probability amplitude of finding a $|D\bar{D}\rangle$ state with s certain quantum number in a physical π_n.[2]

The matrix element in (28) can be further expressed as

$$\begin{aligned}&\langle D_{n_1}(x_1P^+)\bar{D}_{n_2}(x_2P^+)|V_{\text{charm}}|\pi_n(P^+)\rangle \\ &= \frac{2\pi}{P^+}\delta(x_1+x_2-1)\Gamma_{n,n_1,n_2}(x_1,x_2),\end{aligned} \tag{29}$$

where $x_i = k_i^+/P^+$ $(i = 1, 2)$ is the $+$ momentum fraction of $D, \bar{D}$ with respect to π_n, and this matrix element vanishes unless the light-cone momentum conservation is satisfied. The transition vertex function Γ was first given by Callan, Coote, and Gross long ago [30], and its explicit form reads

$$\begin{aligned}\Gamma_{n,n_1,n_2}(x_1,x_2) = 4\lambda\sqrt{\frac{\pi}{N_c}}\Bigg[&\int_{x_1}^1 dy_1\int_0^{x_1}dy_2\frac{1}{(y_2-y_1)^2} \\ &\times\varphi_n^{u\bar{u}}(1-y_1)\varphi_{n_1}^{c\bar{u}}\left(1-\frac{y_2}{x_1}\right)\varphi_{n_2}^{u\bar{c}}\left(\frac{1-y_1}{x_2}\right) \\ &-\int_{x_2}^1 dy_1\int_0^{x_2}dy_2\frac{1}{(y_2-y_1)^2} \\ &\times\varphi_n^{u\bar{u}}(y_1)\varphi_{n_2}^{u\bar{c}}\left(\frac{y_2}{x_2}\right)\varphi_{n_1}^{c\bar{u}}\left(\frac{y_1-x_2}{x_1}\right)\Bigg].\end{aligned} \tag{30}$$

In Fig. 1 we present some schematic diagrams depicting the triple-meson vertex Γ.

It should be emphasized that the charm and anticharm quarks are generated nonperturbatively and hadronized into the D and $\bar{D}$ mesons. This nonperturbative process is represented by the exchange of an infinite number of gluons between the c $(\bar{c})$ quark and $\bar{u}$ (u) quark, as shown in Fig. 2. It is the charm quark inside the D meson that is later "probed" and gives rise to the charm-quark PDF. Therefore, the charm quark in our calculation is genuinely intrinsic.

It is reassuring to see that the vertex function Γ is indeed of order $N_c^{-1/2}$. At first sight, one may worry that the Γ may become divergent when the integration variables approach the boundary, i.e., $y_1, y_2 \to x_1$ or x_2. A careful look reveals that, near the boundary, both terms in the integrand are simultaneously approaching $\varphi_n^{u\bar{u}}(x_2)\varphi_{n_1}^{c\bar{u}}(0)\varphi_{n_2}^{u\bar{c}}(1)$, and therefore the potential IR divergences cancel, so the vertex function Γ is IR finite.

Substituting Eqs. (21) and (26) into the PDF definition in (20) and repeatedly using the commutation relation in (14), we can express the intrinsic charm PDF of the π_n as

$$\begin{aligned}f_{c/\pi_n}(x) = \sum_{n_1n_2n_3n_4}\int\frac{dx_1dx_2dx_3dx_4}{16(2\pi)^4x_1x_2x_3x_4}&\tilde{T}_{n,n_1,n_2}(x_1P^+,x_2P^+) \\ &\times\mathcal{H}_{n_3,n_4}^{n_1,n_2}(x_1,x_2,x_3,x_4,x)\tilde{T}_{n,n_3,n_4}^*(x_3P^+,x_4P^+),\end{aligned} \tag{31}$$

[2]Note that we have dropped the $i\epsilon$ term in the energy denominator in (28), because the energy denominator always has a positive sign due to $P^+ \geq k_i^+$, $k_j^+ \geq 0$ and $\mu_D, \mu_{\bar{D}} \gg \mu_\pi$, if we do not consider the excessively highly excited pion.

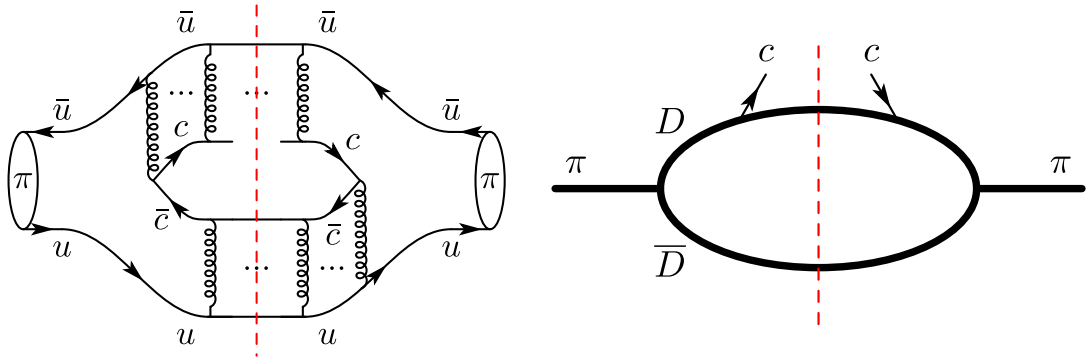

FIG. 2. Schematic figures for our results of the intrinsic charm PDF of π (left) and for the MCM (right).

with

$$\begin{aligned}\mathcal{H}^{n_1,n_2}_{n_3,n_4}(x_1,x_2,x_3,x_4,x) &\equiv \int \frac{dz^-}{4\pi} e^{-ixP^+z^-}\langle D_{n_3}(x_3P^+)\bar{D}_{n_4}(x_4P^+)|c^\dagger_R(z^-)c_R(0)|D_{n_1}(x_1P^+)\bar{D}_{n_2}(x_2P^+)\rangle \\ &= 4\pi\Bigg[\delta_{n_2n_4}x_2\delta(x_4-x_2)\theta(x)\theta(x_3-x)\varphi^{c\bar{u}}_{n_3}\left(\frac{x}{x_3}\right)\varphi^{c\bar{u}}_{n_1}\left(\frac{x+x_1-x_3}{x_1}\right) \\ &\quad -\delta_{n_1n_3}x_1\delta(x_3-x_1)\theta(-x)\theta(x_2+x)\varphi^{u\bar{c}}_{n_2}\left(\frac{x+x_2}{x_2}\right)\varphi^{u\bar{c}}_{n_4}\left(\frac{x+x_2}{x_4}\right)\Bigg],\end{aligned} \tag{32}$$

in which the $\theta(x)$ and $\theta(-x)$ terms represent the charm and anticharm sectors, respectively.

The result in Eq. (33) can be obtained through a diagrammatic approach by introducing the three-meson vertex and the meson-$q\bar{q}$ vertex. We present the calculation using the diagrammatic approach in the Appendix. This diagrammatic approach also indicates that the charm quark in our calculation is intrinsic.

Substituting the definition of $\tilde{T}$ in (28) into (31), we finally arrive at a compact form of the intrinsic charm PDF of the π_n:

$$\begin{aligned}f_{c/\pi_n}(x) &= \sum_{n_1,n_2,n_3,n_4}\int dx_1 \frac{\Gamma_{n,n_1,n_2}(x_1,1-x_1)\Gamma^*_{n,n_3,n_4}(x_1,1-x_1)}{16\pi x_1(1-x_1)}\left(\frac{\mu^2_{D_{n_1}}}{2x_1}+\frac{\mu^2_{\bar{D}_{n_2}}}{2(1-x_1)}-\frac{\mu^2_{\pi_n}}{2}\right)^{-1} \\ &\quad\times\left(\frac{\mu^2_{D_{n_3}}}{2x_1}+\frac{\mu^2_{\bar{D}_{n_4}}}{2(1-x_1)}-\frac{\mu^2_{\pi_n}}{2}\right)^{-1}\Bigg[\frac{\theta(x)\theta(x_1-x)}{x_1}\delta_{n_2n_4}\varphi^{c\bar{u}}_{n_3}\left(\frac{x}{x_1}\right)\varphi^{c\bar{u}}_{n_1}\left(\frac{x}{x_1}\right) \\ &\quad-\frac{\theta(-x)\theta(x-x_1+1)}{1-x_1}\delta_{n_1n_3}\varphi^{u\bar{c}}_{n_2}\left(1+\frac{x}{1-x_1}\right)\varphi^{u\bar{c}}_{n_4}\left(1+\frac{x}{1-x_1}\right)\Bigg].\end{aligned} \tag{33}$$

Equation (33) is the main result of this work, which represents the field-theoretical expression for the intrinsic charm PDF of a light meson in the 't Hooft model. A schematic Feynman diagram to visualize this formula is shown in the left diagram of Fig. 2. The most important message is that there is an infinite tower of charmed mesons and anticharmed mesons that manifest as the higher Fock components of a light meson and contribute to the intrinsic charm PDF. Note that the principle quantum numbers n_1, n_2, n_3, and n_4 in the sum over (anti)charmed mesons are all independent. It is worth mentioning that, if we only keep the diagonal terms in the sum, i.e., we take $n_1 = n_3$ and $n_2 = n_4$ simultaneously, Eq. (33) reduces to the prediction of the intrinsic charm PDF from the MCM. We will discuss the derivation of the intrinsic charm PDF in the MCM in detail in the next section.

IV. THE BHPS MODEL AND MCM IN QCD$_2$

The BHPS model is a very simple and intuitive model to parametrize the intrinsic charm PDF of a light hadron. The key assumption is that the four-quark Fock component $|u\bar{u}c\bar{c}\rangle$ in π can be treated as a free four-body state [2,3]. The intrinsic charm PDF can then be approximated from the transition probability of $|\pi\rangle \to |u\bar{u}c\bar{c}\rangle$ by the first-order light-front perturbation theory:

$$\frac{d\text{Prob}}{dx_u dx_{\bar{u}} dx_c dx_{\bar{c}}} \propto \delta(1-x_u-x_{\bar{u}}-x_c-x_{\bar{c}}) \times \left(m_\pi^2-\frac{m_u^2}{x_u}-\frac{m_{\bar{u}}^2}{x_{\bar{u}}}-\frac{m_c^2}{x_c}-\frac{m_{\bar{c}}^2}{x_{\bar{c}}}\right)^{-2}, \quad (34)$$

where x_i indicates the $+$ momentum fraction carried by each parton.

In the heavy-quark limit $m_c \gg m_u, m_\pi$, one can drop small quantities in the energy denominator, and (34) reduces to

$$\frac{d\text{Prob}}{dx_u dx_{\bar{u}} dx_c dx_{\bar{c}}} \propto \delta(1-x_u-x_{\bar{u}}-x_c-x_{\bar{c}}) \left(\frac{x_c x_{\bar{c}}}{x_c+x_{\bar{c}}}\right)^2. \quad (35)$$

Integrating (35) over x_u, $x_{\bar{u}}$, $x_{\bar{c}}$, one then arrives at the intrinsic charm PDF predicted by the BHPS model:

$$f_c(x) = Ax^2\left[\frac{1}{2}(1+4x-5x^2)+x(2+x)\ln x\right], \quad (36)$$

where A is an unknown normalization constant which cannot be determined within the BHPS model itself. There are three popular variants of the BHPS model. The BHPS1 and BHPS2 models determine the parameter A through different global fit recipes, and the BHPS3 model takes numerical integration directly following (34) [1]. Inspired by the ansatz of the BHPS model, Pumplin parametrized the intrinsic charm PDF of a proton using a five-quark model including quarks' transverse motion [31].

Another influential model is the MCM which assumes that the proton has non-negligible five-quark Fock component composed of a charmed baryon and a charmed meson due to inevitable quantum fluctuation [15–17]. In the context of the current work, the relevant quantum fluctuation inside π is the higher Fock component composed of the charmed and anticharmed mesons. According to the spirit of the MCM, the intrinsic charm PDF of the π_n is expressed as the transition probability of $\pi_n \to D_{n_1}\bar{D}_{n_2}$ convoluted with the valence charm PDF inside the charmed meson D_{n_1}:

$$f_{c/\pi_n}(x) = \sum_{n_1,n_2}\int_0^1 dy \mathcal{F}_{n,n_1,n_2}(y)\int_0^1 d\eta f_{c/D_{n_1}}(\eta)\delta(x-\eta y) = \sum_{n_1,n_2}\int_x^1 \frac{dy}{y}\mathcal{F}_{n,n_1,n_2}(y) f_{c/D_{n_1}}\left(\frac{x}{y}\right), \quad (37)$$

where $\mathcal{F}_{n,n_1,n_2}(y)$ denotes the transition probability of π_n with $+$ momentum P^+ transitioning into a charmed meson D_{n_1} that carries the $+$ momentum yP^+, and $f_{c/D_{n_i}}(x)$ denotes the valence charm PDF of the charmed meson D_{n_i}.

Let us first consider the transition probability factor $\mathcal{F}$ accompanied with the process $\pi_n \to D_{n_1}(x_1), \bar{D}_{n_2}$:

$$\mathcal{F}_{n,n_1n_2}(x_1)dx_1 = \frac{1}{\tilde{V}}\frac{1}{2P^+}\frac{P^+dx_1}{(2\pi)(2x_1P^+)} \times \int \frac{P^+dx_2}{(2\pi)(2x_2P^+)}|\langle D_{n_1}(x_1P^+) \times \bar{D}_{n_2}(x_2P^+)|\pi_n'(P^+)\rangle|^2. \quad (38)$$

Note that the inner product in (38) is exactly the $\tilde{T}$ function defined in (28), which characterizes the probability amplitude of finding a specific $D\bar{D}$ state inside the π_n. Since we do not care about the anticharmed meson $\bar{D}_{n_2}$, a phase-space integration should be assigned to the $+$ momentum fraction x_2 carried by the $\bar{D}_{n_2}$ meson. However, as indicated in (29), $+$ momentum conservation demands that the $\tilde{T}$ function contains a δ function $\delta(1-x_1-x_2)$. Therefore, the integration over x_2 becomes trivial. Interestingly, the factor $1/\tilde{V}$ can help eliminate the ill-defined $\delta(0)$ arising from squaring the $\tilde{T}$ function, since the finite volume $\tilde{V}$ can be identified with $2\pi\delta_V(0\times P^+)$ in the box quantization.

Substituting (28) and (29) into (38), it is straightforward to obtain

$$\mathcal{F}_{n,n_1n_2}(x_1) = \frac{1}{16\pi}\frac{1}{x_1(1-x_1)}\frac{|\Gamma_{n,n_1n_2}(x_1,1-x_1)|^2}{\left(\frac{\mu_{D_{n_1}}^2}{2x_1}+\frac{\mu_{\bar{D}_{n_2}}^2}{2(1-x_1)}-\frac{\mu_{\pi_n}^2}{2}\right)^2}. \quad (39)$$

In passing, we emphasize that, in addition to the intrinsic charm PDF, one can also deuce the intrinsic anticharm PDF from (33), since it satisfies the relation $f_{\bar{c}/\pi}(x) = -f_{c/\pi}(-x)$ due to the charge-conjugation symmetry inherent in the PDF definition (20) for a neutral π meson. In order to make an intimate comparison between the MCM prediction and our results in (33), the anticharm sector should also be explicitly added to the MCM, and hence we generalize (37) as

$$f_{c/\pi_n}(x) = \sum_{n_1,n_2}\int_0^1 dy\left(\mathcal{F}_{n,n_1,n_2}(y)\int_0^1 d\eta f_{c/D_{n_1}}(\eta)\delta(x-\eta y) - \mathcal{F}_{n,n_1,n_2}(1-y)\int_0^1 d\eta f_{\bar{c}/\bar{D}_{n_2}}(\eta)\delta(-x-\eta y)\right) = \sum_{n_1,n_2}\int_0^1 dy\mathcal{F}_{n,n_1,n_2}(y)\left(\theta(x)\theta(y-x)\frac{f_{c/D_{n_1}}\left(\frac{x}{y}\right)}{y} - \theta(-x)\theta(x-y+1)\frac{f_{\bar{c}/\bar{D}_{n_2}}\left(-\frac{x}{1-y}\right)}{1-y}\right)$$

$$= \sum_{n_1,n_2} \int_0^1 dy \mathcal{F}_D(y) \left(\theta(x)\theta(y-x) \frac{1}{y} \left[\varphi_{n_1}^{c\bar{u}} \left(\frac{x}{y} \right) \right]^2 - \theta(-x)\theta(x-y+1) \frac{1}{1-y} \left[\varphi_{n_2}^{u\bar{c}} \left(1 + \frac{x}{1-y} \right) \right]^2 \right). \tag{40}$$

In (40) we have made use of the knowledge that the valence charm PDF inside a D meson is simply the square of the corresponding 't Hooft wave function:

$$f_{c/D_n}(x) = [\varphi_n^{c\bar{u}}(x)]^2, \tag{41a}$$

$$f_{\bar{c}/\bar{D}_n}(x) = f_{u/\bar{D}_n}(1-x) = [\varphi_n^{u\bar{c}}(1-x)]^2. \tag{41b}$$

Plugging (39) into (40), we obtain the final prediction of the intrinsic charm PDF given by the MCM,

$$f_{c/\pi_n}(x) = \sum_{n_1,n_2} \int dx_1 \frac{|\Gamma_{n,n_1n_2}(x_1, 1-x_1)|^2}{16\pi x_1(1-x_1)} \left(\frac{\mu_{D_{n_1}}^2}{2x_1} + \frac{\mu_{\bar{D}_{n_2}}^2}{2(1-x_1)} - \frac{\mu_{\pi_n}^2}{2} \right)^{-2} \times \left(\theta(x)\theta(x_1-x) \frac{\left[\varphi_{n_1}^{c\bar{u}} \left(\frac{x}{x_1} \right) \right]^2}{x_1} - \theta(-x)\theta(x-x_1+1) \frac{\left[\varphi_{n_2}^{u\bar{c}} \left(1 + \frac{x}{1-x_1} \right) \right]^2}{1-x_1} \right). \tag{42}$$

A schematic Feynman diagram to illustrate the MCM is shown in the right diagram of Fig. 2.

It is amazing that the MCM prediction of the intrinsic charm PDF looks quite similar to our results in (33), except that the latter does not enforce the diagonal condition $n_1 = n_3$ and $n_2 = n_4$, and the "interference" terms with $n_1 \neq n_3$ or $n_2 \neq n_4$ in (33) do make important contributions.

It is interesting to note that, because of the orthogonality relation of the 't Hooft wave functions as in (15), the "interference" terms do not contribute to the first Mellin moment of the intrinsic charm PDF. Of course, they will affect the shape of the intrinsic charm PDF and the average charm momentum fraction.

V. NUMERICAL RESULTS

In this section, we present the numerical results of the intrinsic charm PDF in a fictitious pion meson. In the large-N_c limit, we set the mass scale following the ansatz in Ref. [32] by choosing the value of the 't Hooft coupling $\sqrt{2\lambda} = 340$ MeV in correspondence to the value of the string tension in realistic QCD. To save calculational labor, we deliberately choose the up-quark mass $m_u = 0.749\sqrt{2\lambda}$, which is equal to the strange-quark mass determined in [33]. We also study the intrinsic charm content inside a pion with different values of the charm-quark mass. The charm mass is varied from $m_c = 4.19\sqrt{2\lambda}$ to $m_c = 3m_b$, with $m_b = 13.66\sqrt{2\lambda}$. For the details of setting masses of different quark flavors, we refer interested readers to Refs. [33,34].

The light-cone wave functions of the $u\bar{u}$, $u\bar{c}$, and $c\bar{u}$ states are obtained by solving the 't Hooft equation by means of the Brower-Spence-Weis (BSW) method [35]. We use 120 BSW bases for the cases $m_c < 13.66\sqrt{2\lambda}$, 192 BSW bases for $13.66\sqrt{2\lambda} \leq m_c \leq 27.32\sqrt{2\lambda}$, and 264 BSW bases for $m_c > 27.32\sqrt{2\lambda}$.

We calculate the intrinsic charm PDF according to our field-theoretical expression (33), as well as the predictions given by the MCM and the BHPS model. To make a fair comparison, we normalize the predictions of the BHPS model such that its first Mellin moment is identical to that from our results in (33) and MCM prediction in (42). In our analysis we also include a naive MCM, which only includes the ground state in the sum in (42).

The intrinsic charm PDF from our 't Hooft model calculation in (33) and the MCM (42) involve a sum over all possible intermediate meson states. We impose a truncation $n_{1,2,3,4} \leq N$ to facilitate the summation. Due to the limitation of our computing resources, the maximum value of N is set to $N_{\max} = 60$. The convergence criteria is set by searching for the lowest $N = N_0$ that satisfies

$$\frac{\int_0^1 dx [f_c^{(N)}(x) - f_c^{(N_{\max})}(x)]^2}{\int_0^1 dx \left[\frac{f_c^{(N)}(x) + f_c^{(N_{\max})}(x)}{2} \right]^2} \leq 0.01, \tag{43}$$

where $f_c^{(N)}(x)$ denotes the intrinsic charm PDF in Eq. (33) with summation truncated at N. For instance, the intrinsic charm PDF of the first excited pion converges at $N_0 = 34$ when $m_c = 4.19\sqrt{2\lambda}$ and $N_0 = 48$ when $m_c = 13.66\sqrt{2\lambda}$. The intrinsic PDF from the MCM shows a better converge tendency, and thus we take $N = N_{\max}$ as the final results for the MCM.

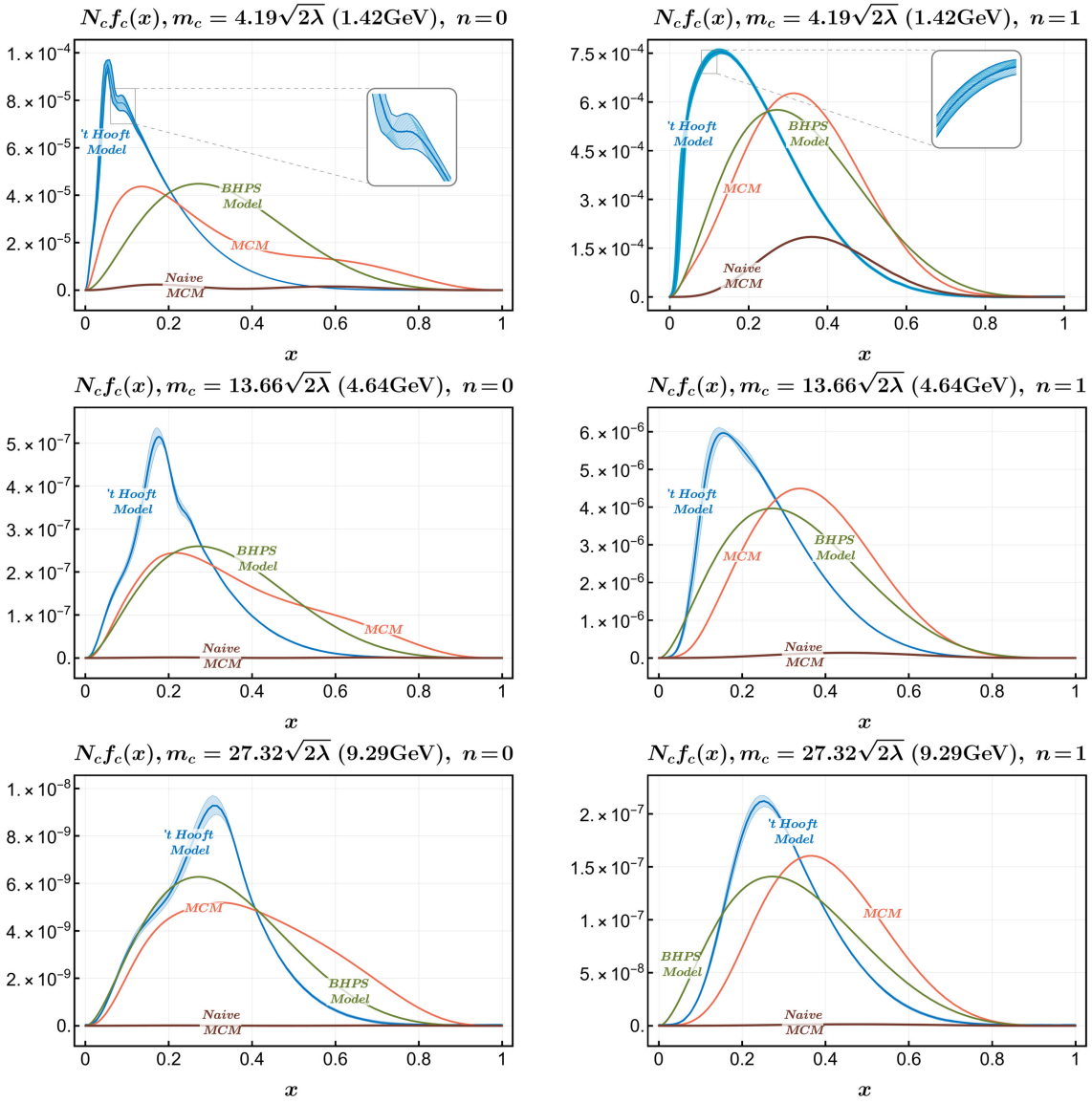

FIG. 3. Intrinsic charm PDF in the pion from our analysis ('t Hooft model), the MCM, a naive MCM, and the BHPS models. We show the results with some representative values of charm-quark masses. The left and right columns show the results of a ground state and first excited state π, respectively. The thin dark blue curves in the windows correspond to each N lying between N_0 and 60.

The contribution from high excited states in Eq. (33) only affects the microscopic texture of the intrinsic charm PDF. We treat the choices of N as the source of systematic uncertainties in our calculation. To be more specific, we plot the envelopes of curves corresponding to the quark PDF with $N_0 \leq N \leq N_{\max}$ and use the upper and lower envelopes as upper and lower bounds, respectively. The central value is given as the average of the upper and lower bounds. To demonstrate how to determine the upper and lower bounds, we magnify part of the curve corresponding to our results in the first row of Fig. 3.

In Fig. 3 we present the intrinsic charm PDF from our expression rigorously derived from the 't Hooft model with three different choices of charm masses. The results of the BHPS model, MCM, and naive MCM are also juxtaposed for comparison. We plot the results of both the ground-state and the first excited pions. We find that the profiles of our results significantly differ from the predictions given by the MCM and the BHPS model. The results of the naive MCM are 1–2 orders of magnitude smaller than the other results. This comparison clearly shows that one cannot simply ignore the contribution from the excited charmed meson states when applying the MCM in phenomenological studies. It may cast some doubt on the phenomenological work of the intrinsic charm PDF in a nucleon [17]. Our calculation shows that it is crucial to include the contributions from the "interference" terms between mesons with different principle quantum numbers. This may provide some useful guidance on the optimized parametrization of the intrinsic charm content from the MCM.

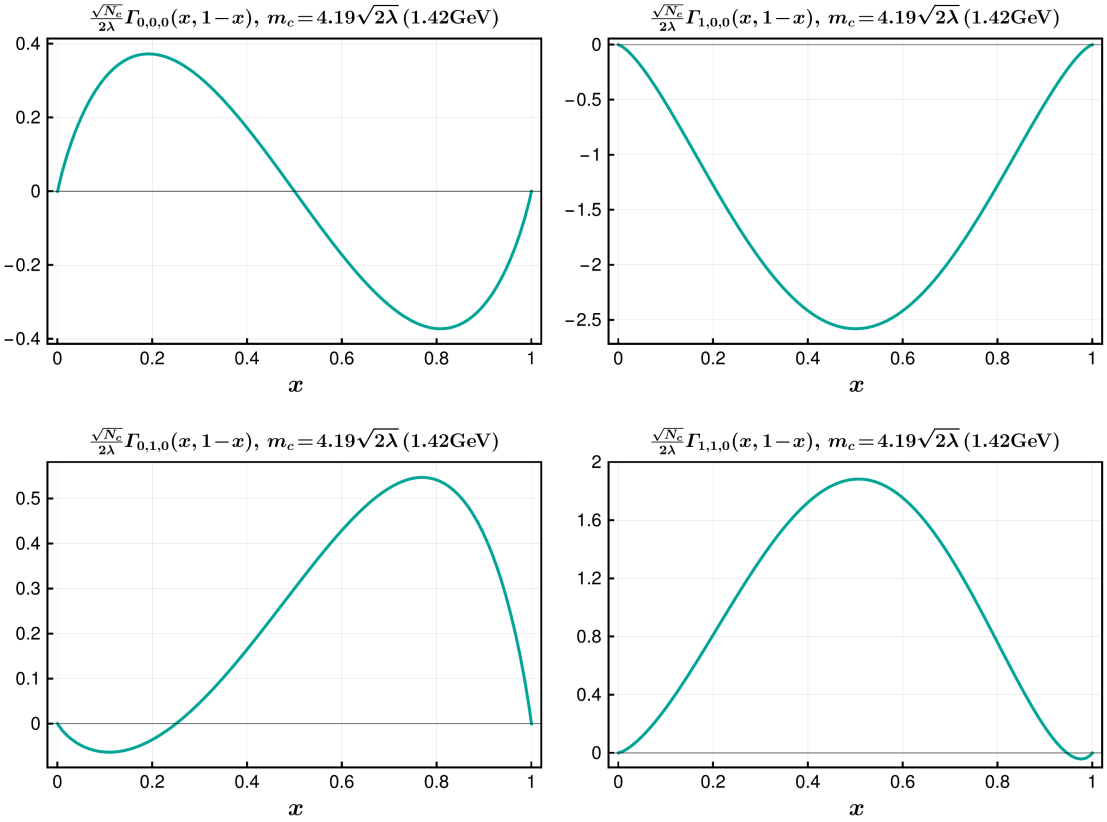

FIG. 4. Transition vertex function $\Gamma_{n,n_1,n_2}(x,1-x)$. We plot two typical cases, i.e., $n_1=n_2=0$ and $n_1=1$, $n_2=0$ for $n=0$ (left column) and $n=1$ (right column).

The intrinsic charm PDF of the first excited π is about 1 order of magnitude larger than that of the lowest-lying pion. Actually, this can be reflected at the level of the transition vertex function. In Fig. 4, we compare the transition vertex function $\Gamma_{n,n_1,n_2}(x,1-x)$ between the ground state and the first excited state. We observe that the transition vertex function with $n=1$ is significantly larger in magnitude than the $n=0$ case. This difference might be due to the distinct charge-conjugation properties. Recall the charge-conjugate transformation of the mesonic annihilation operator

$$\mathcal{C}m_n^{u\bar{u}}(P^+)\mathcal{C}^{-1}=(-1)^{n+1}m_n^{u\bar{u}}(P^+), \tag{44}$$

where $\varphi_n^{u\bar{u}}(x)=(-1)^n\varphi_n^{u\bar{u}}(1-x)$ has been applied. The ground state and the first excited pion state have opposite C parities. For a pion transitioning into $|D_{n_1}(k_1^+)\bar{D}_{n_2}(k_2^+)\rangle$, when $n_1=n_2$ and $k_1^+=k_2^+$, the final state has an even C parity, and thus this is only possible if the initial pion is the first excited state. Correspondingly, $\Gamma_{0,0,0}$ vanishes at $x_1=x_2=\frac{1}{2}$. As the vertex function is continuous, the charge-conjugate symmetry leads to the suppression of the ground-state transition at all x_1, as shown in Fig. 4.

We also find that when we increase the charm-quark mass, the peak position of our result tends to shift to a larger x value. The peak position of the MCM remains almost unchanged. Meanwhile, the magnitude of the intrinsic charm PDF from all model predictions decreases very fast with increasing charm mass.

To quantitatively investigate how the intrinsic charm PDF depends on the charm-quark mass, we also calculate the first two Mellin moments of the intrinsic charm PDF:

$$\langle x^0\rangle=\int_0^1 dx\, f_c(x),\qquad \langle x^1\rangle=\int_0^1 dx\, x f_c(x). \tag{45}$$

The first two moments have straightforward interpretations: the first moment corresponds to the average number of charm quarks inside the pion, while the second moment characterizes the average momentum fraction carried by the charm. We vary the charm-quark mass from $4.19\sqrt{2\lambda}$ to $40.98\sqrt{2\lambda}$. The numerical results of the first two Mellin moments are shown in Table I.

We use a simple power-law ansatz $\langle x^0\rangle,\langle x^1\rangle\propto m_c^{-d}$ and fit the moments in the large-charm-mass region. We vary the fitting range[3] from $18.17\sqrt{2\lambda}\le m_c\le 40.98\sqrt{2\lambda}$ to

[3]The calculation with a mass beyond $m_c=40.98\sqrt{2\lambda}$ becomes numerically unstable, and thus we stop pursuing the extremely heavy charm-quark cases.

TABLE I. First and second Mellin moments of the intrinsic charm PDF and their ratios. The results of the ground-state ($n = 0$) and the first excited state ($n = 1$) pion are provided. The charm-quark masses are given in units of $\sqrt{2\lambda}$ and GeV.

$n = 0$						
$m_c[\sqrt{2\lambda}(\mathrm{GeV})]$	4.19 (1.42)	5.51 (1.87)	6.53 (2.22)	7.55 (2.57)	8.57 (2.91)	9.58 (3.26)
$\langle x^0\rangle$	1.86×10^{-5}	6.26×10^{-6}	3.09×10^{-6}	1.67×10^{-6}	9.71×10^{-7}	5.78×10^{-7}
$\langle x^1\rangle$	2.81×10^{-6}	1.03×10^{-6}	5.38×10^{-7}	3.04×10^{-7}	1.83×10^{-7}	1.15×10^{-7}
$\langle x^1\rangle/\langle x^0\rangle$	0.151	0.164	0.174	0.183	0.189	0.200
$m_c[\sqrt{2\lambda}(\mathrm{GeV})]$	10.60 (3.61)	11.62 (3.95)	12.64 (4.30)	13.66 (4.64)	18.17 (6.18)	22.81 (7.76)
$\langle x^0\rangle$	3.63×10^{-7}	2.36×10^{-7}	1.58×10^{-7}	1.10×10^{-7}	2.45×10^{-8}	7.12×10^{-9}
$\langle x^1\rangle$	7.52×10^{-8}	5.09×10^{-8}	3.50×10^{-8}	2.51×10^{-8}	6.36×10^{-9}	2.01×10^{-9}
$\langle x^1\rangle/\langle x^0\rangle$	0.207	0.216	0.222	0.230	0.259	0.283
$m_c[\sqrt{2\lambda}(\mathrm{GeV})]$	27.32 (9.29)	32.16 (10.93)	37.00 (12.58)	40.98 (13.93)		
$\langle x^0\rangle$	2.56×10^{-9}	9.80×10^{-10}	4.24×10^{-10}	2.27×10^{-10}		
$\langle x^1\rangle$	7.74×10^{-10}	3.15×10^{-10}	1.42×10^{-10}	7.86×10^{-11}		
$\langle x^1\rangle/\langle x^0\rangle$	0.303	0.320	0.335	0.346		
$n = 1$						
$m_c[\sqrt{2\lambda}(\mathrm{GeV})]$	4.19 (1.42)	5.51 (1.87)	6.53 (2.22)	7.55 (2.57)	8.57 (2.91)	9.58 (3.26)
$\langle x^0\rangle$	2.37×10^{-4}	7.80×10^{-5}	3.89×10^{-5}	2.14×10^{-5}	1.26×10^{-5}	7.79×10^{-6}
$\langle x^1\rangle$	5.15×10^{-5}	1.74×10^{-5}	8.81×10^{-6}	4.92×10^{-6}	2.95×10^{-6}	1.86×10^{-6}
$\langle x^1\rangle/\langle x^0\rangle$	0.218	0.223	0.226	0.230	0.235	0.238
$m_c[\sqrt{2\lambda}(\mathrm{GeV})]$	10.60 (3.61)	11.62 (3.95)	12.64 (4.30)	13.66 (4.64)	18.17 (6.18)	22.81 (7.76)
$\langle x^0\rangle$	5.05×10^{-6}	3.39×10^{-6}	2.34×10^{-6}	1.64×10^{-6}	4.45×10^{-7}	1.46×10^{-7}
$\langle x^1\rangle$	1.22×10^{-6}	8.35×10^{-7}	5.87×10^{-7}	4.20×10^{-7}	1.21×10^{-7}	4.24×10^{-8}
$\langle x^1\rangle/\langle x^0\rangle$	0.242	0.247	0.251	0.256	0.273	0.291
$m_c[\sqrt{2\lambda}(\mathrm{GeV})]$	27.32 (9.29)	32.16 (10.93)	37.00 (12.58)	40.98 (13.93)		
$\langle x^0\rangle$	5.76×10^{-8}	2.41×10^{-8}	1.11×10^{-8}	6.23×10^{-9}		
$\langle x^1\rangle$	1.77×10^{-8}	7.76×10^{-9}	3.72×10^{-9}	2.15×10^{-9}		
$\langle x^1\rangle/\langle x^0\rangle$	0.307	0.322	0.335	0.345		

$32.16\sqrt{2\lambda} \le m_c \le 40.98\sqrt{2\lambda}$, and the fitting results are listed in Table II. The fitting indicates that when choosing a relatively heavier quark mass range, the asymptotic behavior approaches m_c^{-6}. To illustrate the scaling behavior, we multiply the moments $\langle x^0\rangle$ and $\langle x^1\rangle$ by m_c^6, which are plotted in Fig. 5. We observe that in the ground state, $m_c^6\langle x^{0,1}\rangle$ tends to converge when m_c is large enough. For the first excited states, the charm quark is not heavy enough to enter the $m_c \to \infty$ asymptotic region.

TABLE II. Fitting of the first two moments to cm_c^{-d}. We vary the fitting range from $18.17 \le m_c \le 40.98$ to $32.16 \le m_c \le 40.98$. The quark masses are given in units of $\sqrt{2\lambda}$.

Fit to cm_c^{-d}	$18.17 \le m_c \le 40.98$	$22.81 \le m_c \le 40.98$	$27.32 \le m_c \le 40.98$	$32.16 \le m_c \le 40.98$
$n = 0, \langle x^0\rangle$	$d = 5.49$	$d = 5.73$	$d = 5.90$	$d = 6.02$
$n = 0, \langle x^1\rangle$	$d = 5.12$	$d = 5.37$	$d = 5.56$	$d = 5.71$
$n = 1, \langle x^0\rangle$	$d = 4.98$	$d = 5.21$	$d = 5.40$	$d = 5.55$
$n = 1, \langle x^1\rangle$	$d = 4.70$	$d = 4.93$	$d = 5.12$	$d = 5.27$

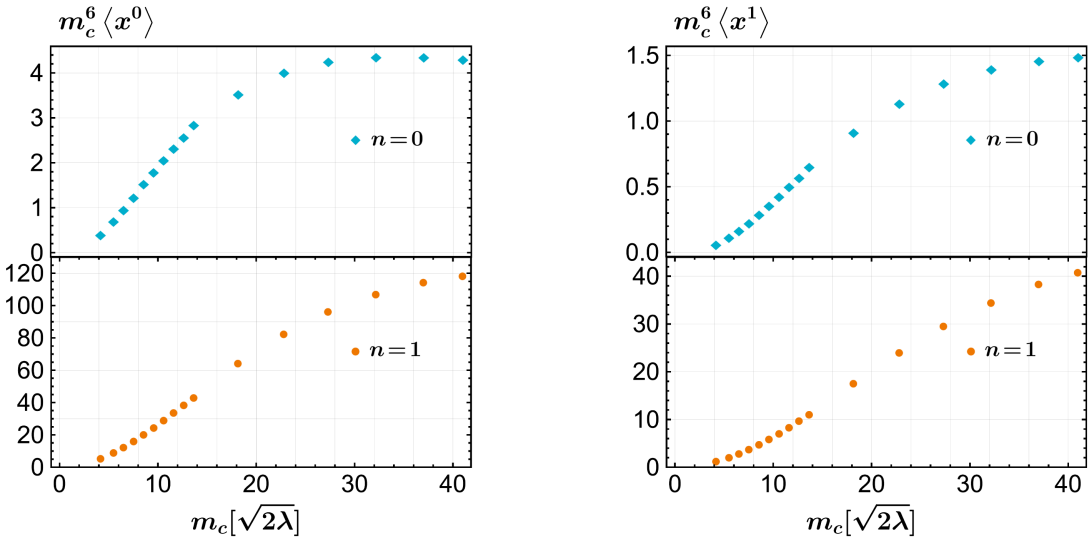

FIG. 5. Intrinsic charm PDF, momentum distribution, and Mellin moments for different charm masses. We multiply by a factor of m_c^6 to compensate for the approximate charm mass scaling factor m_c^{-6} of the moments.

An interesting finding is that, in the heavy-quark limit $m_c \to \infty$, the BHPS model predicts that $\langle x^1\rangle/\langle x^0\rangle = 1/3$ for intrinsic charm [3], while our results show that the ratio reaches $1/3$ at $m_c \approx 37\sqrt{2\lambda}$ and exceeds the BHPS prediction as the charm-quark mass continues to increase. We present the numerical results of $\langle x^1\rangle/\langle x^0\rangle$ in Table I and Fig. 6 for both the ground state and the first excited state of the pion.

VI. SUMMARY

Evidence of the intrinsic charm PDF of a nucleon has recently aroused tremendous interest in the hadron physics community. In this work, following the Collins-Soper operator definition, we carried out a field-theory first-principles study on the intrinsic charm content inside a light neutral meson in the 't Hooft model, i.e., two-dimensional QCD in the large-N_c limit. We explicitly derived the functional form of the intrinsic charm PDF of a light meson in terms of the 't Hooft wave functions of the light meson and an infinite tower of (anti)charmed mesons, which first arises at order $1/N_c$. For the sake of completeness, we also established the functional forms of the intrinsic charm PDF predicted by the two-dimensional versions of the BHPS and meson cloud models. We made a detailed numerical comparison between our results and those model predictions. In particular, we noticed the close relation between our results and the MCM prediction, that is, the "interference" terms omitted in the MCM actually have a non-negligible effect on the shape of the intrinsic charm PDF. We also found that the contributions from excited charmed hadrons are numerically important, which renders the naive MCM (which only considers the lowest-lying charmed hadrons) less trustworthy. Finally, we studied how the intrinsic charm PDF of a light meson depends on the charm-quark mass. The numerical studies revealed that the average charm-quark number and average momentum fraction carried by the charm quark in a light meson drop as m_c^{-6} as the charm-quark mass increases. We hope that our study may shed some light on the nature of the intrinsic charm in the realistic QCD_4.

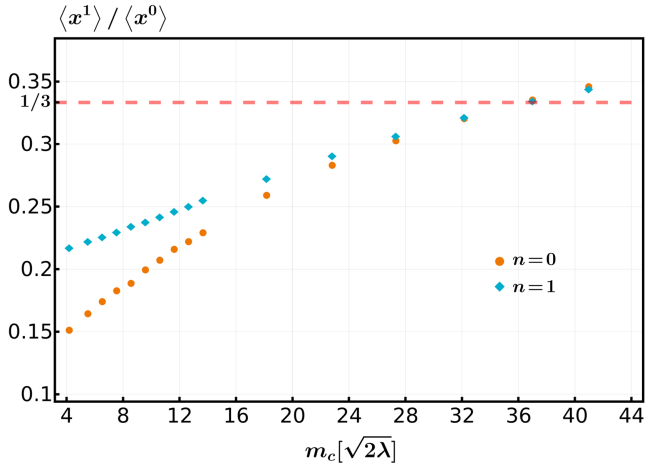

FIG. 6. Ratio $\langle x^1\rangle/\langle x^0\rangle$ from our results. The dashed horizontal line corresponds to the BHPS prediction $\langle x^1\rangle/\langle x^0\rangle = 1/3$. Our result surpasses $1/3$ when $m_c \geq 37\sqrt{2\lambda}$.

ACKNOWLEDGMENTS

This work was supported in part by the High Performance Computing Center of Central South University. The work of S. H., Y. J., and Z. M. is supported in part by the National Natural Science Foundation of China under Grant No. 11925506 and No. 12070131001 (CRC110 by Deutsche Forschungsgemeinschaft). The

work of X.-N. X. and M. L. Z. is supported by the National Natural Science Foundation of China under Grants No. 11905296 and No. 12275364.

APPENDIX: REDERIVING THE INTRINSIC CHARM PDF IN A DIAGRAMMATIC APPROACH

In passing, we note that Eq. (33) can be derived alternatively at the meson level in a diagrammatic approach. The diagram for the intrinsic charm PDF in the pion is shown in Fig. 7 and the intrinsic charm PDF is given by

$$\begin{aligned} f_{c/\pi_n}(x) = & \sum_{n_1,n_2,n_3} \int \frac{d^2k}{(2\pi)^2} \int \frac{d^2p}{(2\pi)^2} \int \frac{d^2p'}{(2\pi)^2} (2\pi)^2 \delta^{(2)}(P-k-p-p') \\ & \times \left[-i\Gamma_{n,n_1n_2}\left(\frac{P^+-k^+}{P^+}, \frac{k^+}{P^+}\right)\right] D^{D_{n_1}}(P-k)\Phi^{c\bar{u}}_{n_1}(p;P-k)S^c(p) \\ & \times (2\pi)\delta(p^+ - xP^+)(2\pi)2p'^+\delta^+\left(p'^2 - m_u^2 + 2\lambda - \frac{2p'^+\lambda}{\rho}\right)(2\pi)\delta^+(k^2-\mu^2_{D,n_2}) \\ & \times \left[i\Gamma^*_{n,n_3n_2}\left(\frac{P^+-k^+}{P^+}, \frac{k^+}{P^+}\right)\right] D^{D_{n_3}*}(P-k)\Phi^{c\bar{u}*}_{n_3}(p,P-k)S^{c*}(p), \end{aligned} \tag{A1}$$

in which the three-meson vertex Γ is defined in Eq. (29) and its explicit form in terms of the 't Hooft wave function is given in Eq. (30). ρ is the artificial IR cutoff regulator introduced in Eq. (8). The first δ function originates from the Fourier factor in the definition of the intrinsic charm PDF (20). The second and third δ functions arise from the cut quark and meson propagators, respectively. $D^{D_n}(P-k)$ denotes the D-meson propagator (D_n in the superscript denotes the nth excited state D meson)

$$D^{D_n}(P-k) = \frac{i}{(P-k)^2 - \mu^2_{D_n} + i\epsilon}, \tag{A2}$$

$S^a(p)$ denotes the dressed quark propagator, whose explicit form is given by [18]

$$S^a(p) = \frac{2ip^+}{p^2 - m_a^2 + 2\lambda - \frac{2p^+\lambda}{\rho} + i\epsilon}, \tag{A3}$$

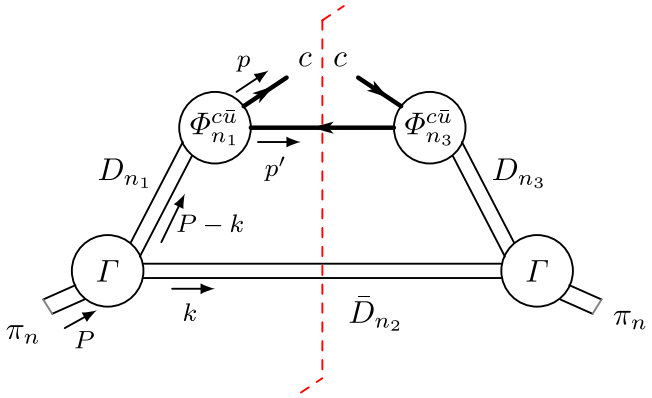

FIG. 7. Diagram at the meson level, in which the dashed line denotes imposing a cut. The superscripts $n_{1,2,3}$ denote the principal quantum number of the meson. The momenta carried by the particles are also presented.

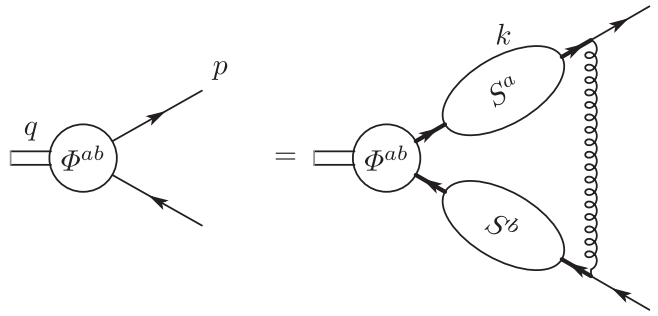

FIG. 8. Diagrammatic representation of the Bethe-Salpeter equation that the meson-$q\bar{q}$ vertex Φ^{ab} satisfies.

and Φ^{ab}_n denotes the meson-$q\bar{q}$ vertex, which satisfies the Bethe-Salpeter equation [36]

$$\begin{aligned} \Phi^{ab}(p;q) = & -2i\lambda \int \frac{dk^2}{(2\pi)^2} \frac{1}{(p^+-k^+)^2} \\ & \times S^a(k)\Phi^{ab}(k;q)S^b(k-q), \end{aligned} \tag{A4}$$

which is represented diagrammatically in Fig. 8. Φ^{ab}_n is related to the meson's 't Hooft wave functions by

$$\begin{aligned} \varphi^{a\bar{b}}_n\left(\frac{p^+}{q^+}\right) = & \int \frac{dp^-}{2\pi} S^a(p)\Phi^{ab}_n(p,q)S^b(p-q) \\ = & -\Phi^{ab}_n(p;q)S^a(p)\big|_{p^-=q^- - \frac{m_b^2-2\lambda}{2(q^+-p^+)} - \frac{2(q^+-p^+)\lambda}{\rho}}, \end{aligned} \tag{A5}$$

where $p^- = q^- - \frac{m_b^2-2\lambda}{2(q^+-p^+)} - \frac{2(q^+-p^+)\lambda}{\rho}$ comes from integrating p^- by taking the residue of[4] $S^b(P-k)$.

[4]Alternatively, one can also choose to taking the residue of $S(P)$, it leads to identical result as Eq. (A5).

It should be noticed that although Eqs. (A1), (A3), and (A5) explicitly depend on the regulator ρ, the ρ dependence will eventually cancel in the final result of $f_{c/\pi_n}(x)$.

Piecing the above together, we get

$$f_{c/\pi_n}(x) = \sum_{n_1,n_2,n_3} \int \frac{dk^+}{2\pi 2k^+} \Gamma_{n,n_1n_2}\left(\frac{P^+-k^+}{P^+}, \frac{k^+}{P^+}\right) \frac{1}{(P-k)^2-\mu^2_{D_{n_1}}} \varphi^{c\bar{u}}_{n_1}\left(\frac{xP^+}{P^+-k^+}\right) \times \Gamma^*_{n,n_3n_2}\left(\frac{P^+-k^+}{P^+}, \frac{k^+}{P^+}\right) \frac{1}{(P-k)^2-\mu^2_{D_{n_3}}} \varphi^{c\bar{u}}_{n_3}\left(\frac{xP^+}{P^+-k^+}\right), \tag{A6}$$

where $P^- = \frac{\mu^2_{\pi_n}}{2P^+}$, $k^- = \frac{\mu^2_{D_{n_2}}}{2k^+}$.

Defining $x_1 \equiv (P^+ - k^+)/P^+$, Eq. (A6) can be written as

$$f_{c/\pi_n}(x) = \sum_{n_1,n_2,n_3} \int \frac{dx_1}{4\pi(1-x_1)} \frac{\Gamma_{n,n_1,n_2}(x_1)}{x_1\left(\mu^2_{\pi_n} - \frac{\mu^2_{D_{n_2}}}{1-x_1}\right) - \mu^2_{D_{n_1}}} \varphi^{c\bar{u}}_{n_1}\left(\frac{x}{x_1}\right) \frac{\Gamma_{n,n_3,n_2}(x_1)}{x_1\left(\mu^2_{\pi_n} - \frac{\mu^2_{D_{n_2}}}{1-x_1}\right) - \mu^2_{D_{n_1}}} \varphi^{c\bar{u}}_{n_3}\left(\frac{x}{x_1}\right), \tag{A7}$$

and it exactly reproduces the charm sector of Eq. (33) in our 't Hooft model calculation result.

[1] T. J. Hou, S. Dulat, J. Gao, M. Guzzi, J. Huston, P. Nadolsky, C. Schmidt, J. Winter, K. Xie, and C. P. Yuan, J. High Energy Phys. 02 (2018) 059.
[2] S. J. Brodsky, P. Hoyer, C. Peterson, and N. Sakai, Phys. Lett. **93B**, 451 (1980).
[3] S. J. Brodsky, C. Peterson, and N. Sakai, Phys. Rev. D **23**, 2745 (1981).
[4] S. J. Brodsky, A. Kusina, F. Lyonnet, I. Schienbein, H. Spiesberger, and R. Vogt, Adv. High Energy Phys. **2015**, 231547 (2015).
[5] J. Blümlein, Phys. Lett. B **753**, 619 (2016).
[6] R. Aaij *et al.* (LHCb Collaboration), Phys. Rev. Lett. **128**, 082001 (2022).
[7] R. D. Ball, A. Candido, J. Cruz-Martinez, S. Forte, T. Giani, F. Hekhorn, K. Kudashkin, G. Magni, and J. Rojo (NNPDF Collaboration), Nature (London) **608**, 483 (2022).
[8] A. Courtoy, J. Huston, P. Nadolsky, K. Xie, M. Yan, and C. P. Yuan, Phys. Rev. D **107**, 034008 (2023).
[9] M. Guzzi, T. J. Hobbs, K. Xie, J. Huston, P. Nadolsky, and C. P. Yuan, Phys. Lett. B **843**, 137975 (2023).
[10] M. Constantinou, A. Courtoy, M. A. Ebert, M. Engelhardt, T. Giani, T. Hobbs, T. J. Hou, A. Kusina, K. Kutak, J. Liang *et al.*, Prog. Part. Nucl. Phys. **121**, 103908 (2021).
[11] R. S. Sufian, T. Liu, A. Alexandru, S. J. Brodsky, G. F. de Téramond, H. G. Dosch, T. Draper, K. F. Liu, and Y. B. Yang, Phys. Lett. B **808**, 135633 (2020).
[12] X. Ji, Phys. Rev. Lett. **110**, 262002 (2013).
[13] X. Ji, Sci. China Phys. Mech. Astron. **57**, 1407 (2014).
[14] X. Ji, Y. S. Liu, Y. Liu, J. H. Zhang, and Y. Zhao, Rev. Mod. Phys. **93**, 035005 (2021).
[15] S. Paiva, M. Nielsen, F. S. Navarra, F. O. Duraes, and L. L. Barz, Mod. Phys. Lett. A **13**, 2715 (1998).
[16] T. J. Hobbs, J. T. Londergan, and W. Melnitchouk, Phys. Rev. D **89**, 074008 (2014).
[17] W. Melnitchouk and A. W. Thomas, Phys. Lett. B **414**, 134 (1997).
[18] G. 't Hooft, Nucl. Phys. **B75**, 461 (1974).
[19] M. Franz, M. V. Polyakov, and K. Goeke, Phys. Rev. D **62**, 074024 (2000).
[20] Y. Jia, S. Liang, X. Xiong, and R. Yu, Phys. Rev. D **98**, 054011 (2018).
[21] K. Kikkawa, Ann. Phys. (N.Y.) **135**, 222 (1981).
[22] A. Nakamura and K. Odaka, Phys. Lett. **105B**, 392 (1981).
[23] S. G. Rajeev, Int. J. Mod. Phys. A **09**, 5583 (1994).
[24] A. Dhar, G. Mandal, and S. R. Wadia, Phys. Lett. B **329**, 15 (1994).
[25] A. Dhar, P. Lakdawala, G. Mandal, and S. R. Wadia, Int. J. Mod. Phys. A **10**, 2189 (1995).
[26] M. Cavicchi, Int. J. Mod. Phys. A **10**, 167 (1995).
[27] J. L. F. Barbon and K. Demeterfi, Nucl. Phys. **B434**, 109 (1995).
[28] K. Itakura, Phys. Rev. D **54**, 2853 (1996).
[29] J. C. Collins and D. E. Soper, Nucl. Phys. **B194**, 445 (1982).
[30] C. G. Callan, Jr., N. Coote, and D. J. Gross, Phys. Rev. D **13**, 1649 (1976).
[31] J. Pumplin, Phys. Rev. D **73**, 114015 (2006).
[32] M. Burkardt, Phys. Rev. D **62**, 094003 (2000).
[33] Y. Jia, S. Liang, L. Li, and X. Xiong, J. High Energy Phys. 11 (2017) 151.
[34] Y. Jia, R. Yu, and X. Xiong, Phys. Rev. D **98**, 074024 (2018).
[35] R. C. Brower, W. L. Spence, and J. H. Weis, Phys. Rev. D **19**, 3024 (1979).
[36] E. E. Salpeter and H. A. Bethe, Phys. Rev. **84**, 1232 (1951).